Supporting material:

Understanding 2p core-level excitons of late transition metals by analysis of mixed-valence copper in a metal–organic framework

Han Wang[a,b,c,*], Gregory M. Su[c,d] Brandon R. Barnett[e,f,†], Walter S. Drisdella[c], Jeffrey R. Long[e,f,g] and David Prendergast[h]

[a]School of Physical Science and Technology, ShanghaiTech University, Shanghai 201210, China

[b]Center for Transformative Science, ShanghaiTech University, Shanghai 201210, China

[c]Chemical Sciences Division, Lawrence Berkeley National Laboratory, Berkeley, CA 94720, USA

[d]Advanced Light Source, Lawrence Berkeley National Laboratory, Berkeley, CA 94720, USA

[e]Materials Sciences Division, Lawrence Berkeley National Laboratory, Berkeley, CA 94720, USA

[f]Department of Chemistry, University of California, Berkeley, Berkeley, CA 94720, USA

[g]Department of Chemical and Biomolecular Engineering, University of California, Berkeley, Berkeley, CA 94720, USA

[h]The Molecular Foundry, Lawrence Berkeley National Laboratory, Berkeley, CA 94720, USA.

† Current Affiliation: Department of Chemistry, University of Rochester, Rochester, New York 14627, USA

[*]Han Wang Email: wanghan3@shanghaitech.edu.cn

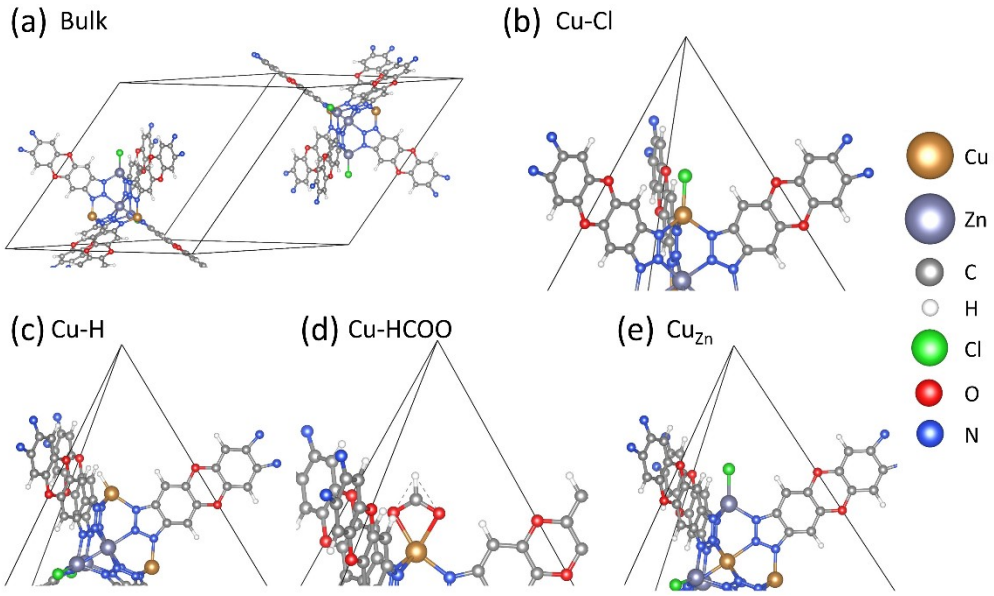

Figure S1. The primitive cell of (a) pristine Cu^{I}-MFU-4*l*, and the primitive cell with defect (b) Cl attached on Cu^{2+} site, (c) H attached on Cu^{2+} site, (d) HCOO group attached on Cu^{2+} site. (e) The primitive cell with two Cu atoms on one node with a Cu_{Zn} defect. The gray, blue, red, green, white, bluish gray and gold balls represent C, N, O, Cl, H, Zn and Cu atoms, respectively.

Table S1. The energy of the first LR-TDDFT root, the electron-hole pair used in the MOM calculation, and the corresponding total energy difference between the MOM shifting energy ($E_{MOM} - E_{GS}$) and TDDFT root energy, respectively. α and β represent the spin up and spin down channels, respectively.

	ωB97M-V		M06-2X	
	Cu^{+}	Cu^{2+}	Cu^{+}	Cu^{2+}
$\epsilon_{LR-TDDFT}^{1st\ root}$ (eV)	925.817	921.563	937.953	928.604
MOM	α 28 →295	β 25→290	α 27→294	β 25→290

$E_{MOM} - E_{GS} - \epsilon_{LR-TDDFT}^{1st\ root}(eV)$	16.145	16.773	3.825	10.238

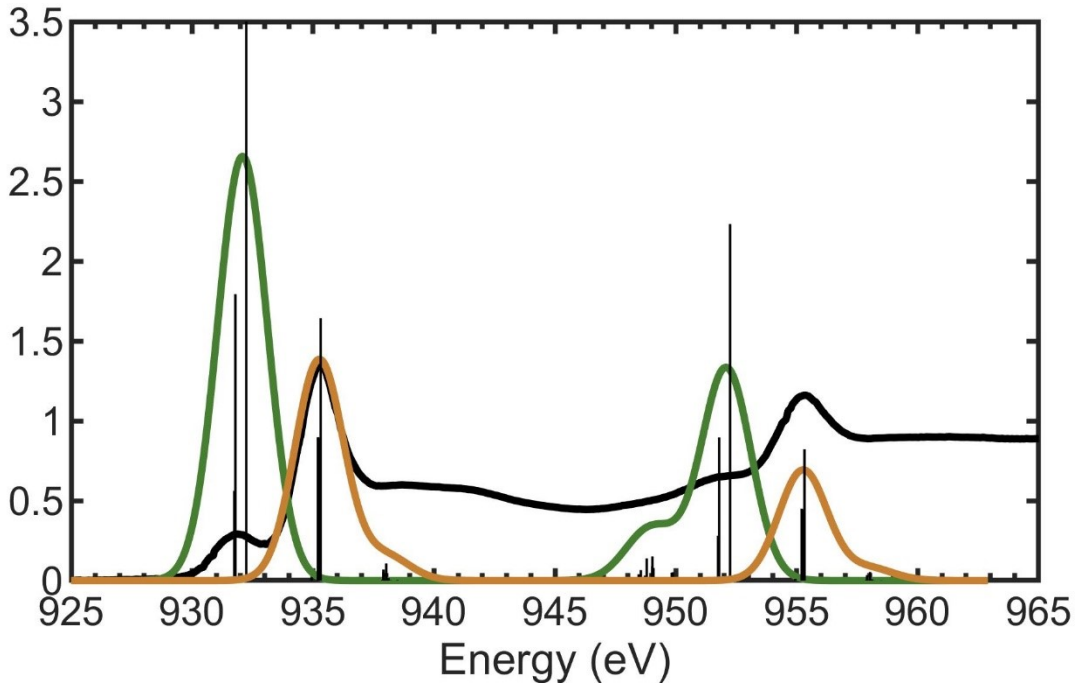

Figure S2. The green and orange curve represent the XAS from Cu^{2+} and Cu^{+} 2p orbitals, respectively. It is calculated with the LR-TDDFT method and the M06-2X functional. The ΔSCF shifts for Cu^{+} and Cu^{2+} spectra are 3.825 eV and 10.238 eV, respectively. The black curve represents the experimental result. The Cu^{2+} is bound to Cl and Cu^{+} has a bound CO molecule.

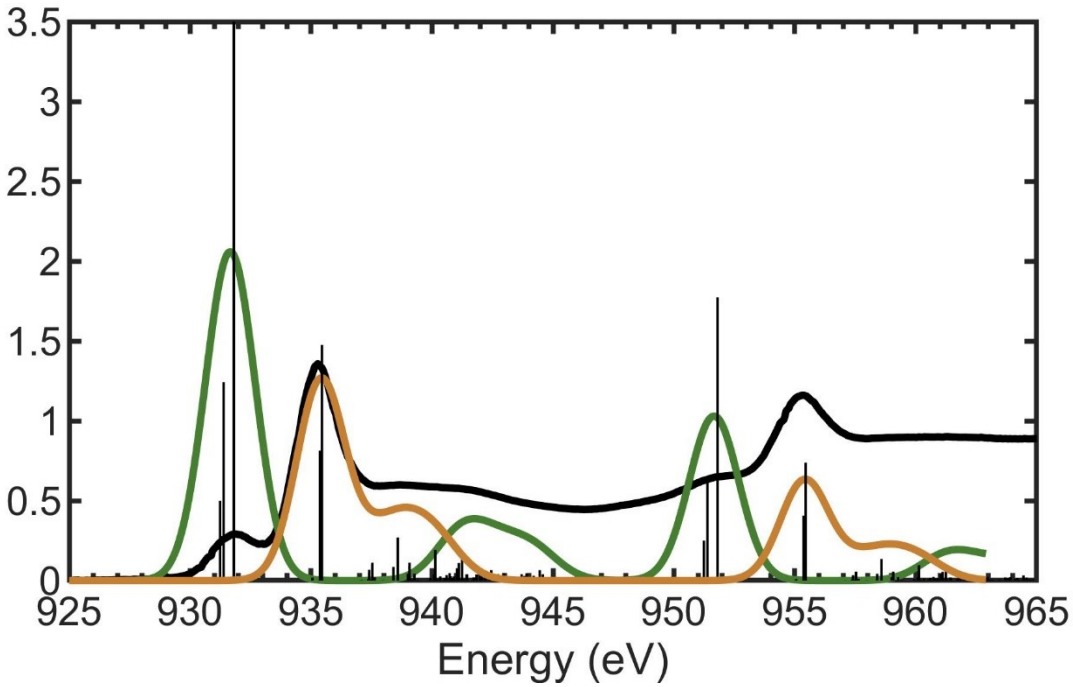

Figure S3. The green and orange curve represent the XAS from Cu^{2+} and Cu^{+} 2p orbitals, respectively. It is calculated with the LR-TDDFT method and the ωB97M-V functional. The ΔSCF shifts for Cu^{+} and Cu^{2+} spectra are 16.145 eV and 16.773 eV, respectively. The black curve represents the experimental result. The Cu^{2+} is bound to Cl and Cu^{+} has a bound CO molecule.

Simulated XAS calculated with the ωB97M-V functional

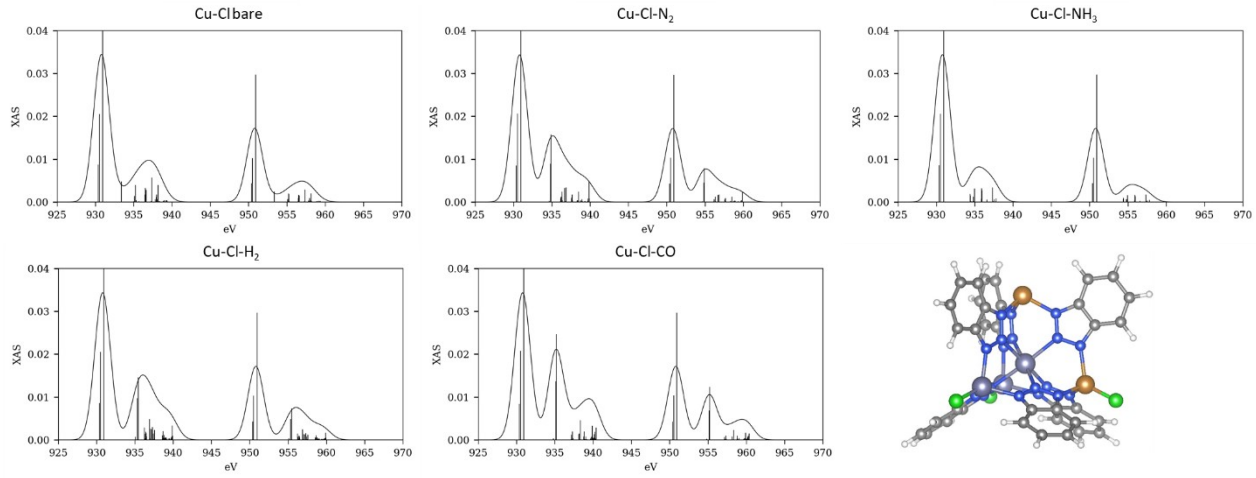

Figure S4. Simulated XAS for two Cu atoms in a cluster with one Cu-Cl defect (Cu-Cl bare), and with various adsorbed molecules: nitrogen (Cu-Cl-N_2); ammonia (Cu-Cl-NH_3); hydrogen (Cu-Cl-H_2); and carbon monoxide (Cu-Cl-CO).

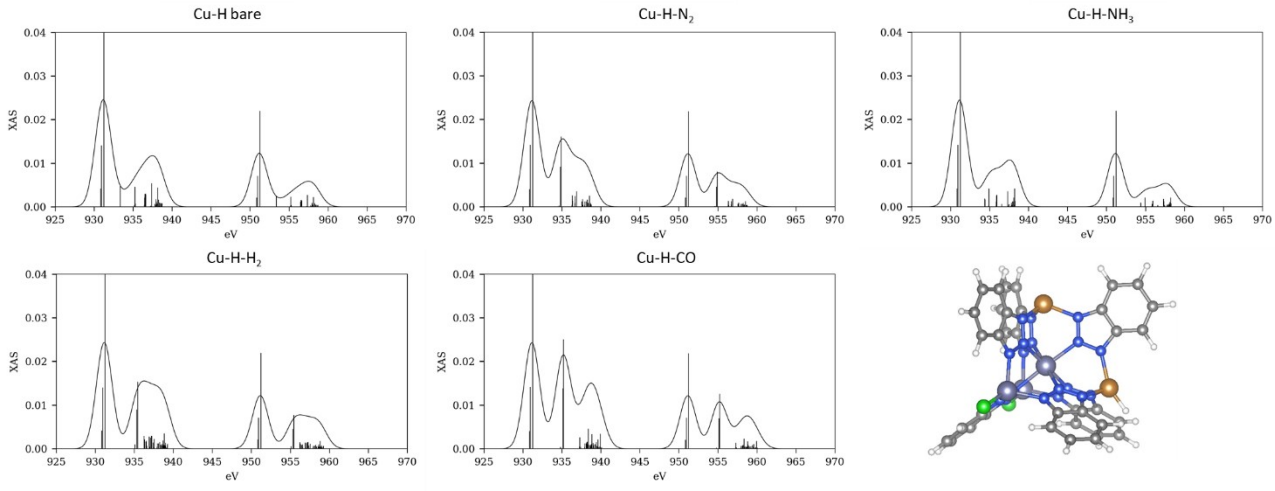

Figure S5. Simulated XAS for two Cu atoms in a cluster with one Cu-H defect and various adsorbed molecules (as for Fig. S4).

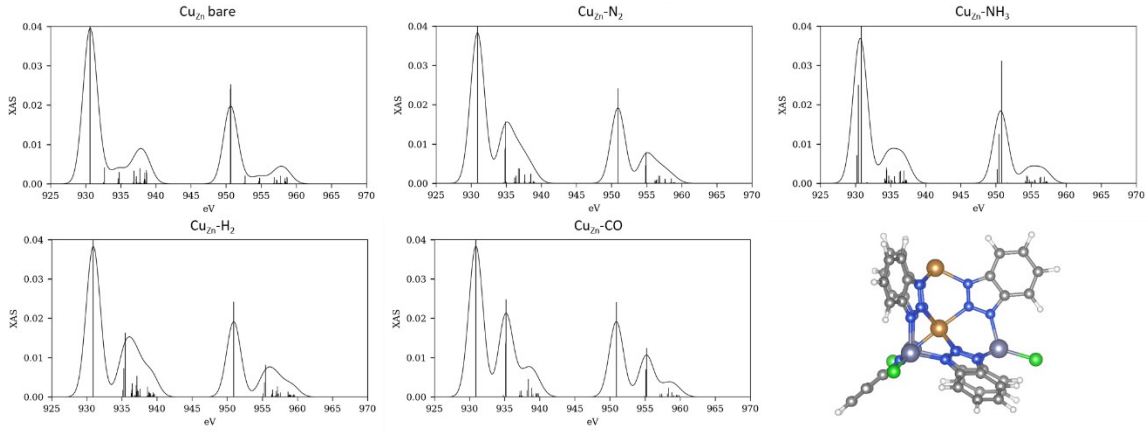

Figure S6. Simulated XAS for two Cu atoms in a cluster with one Cu_{Zn} defect and various adsorbed molecules (as for Fig. S4).

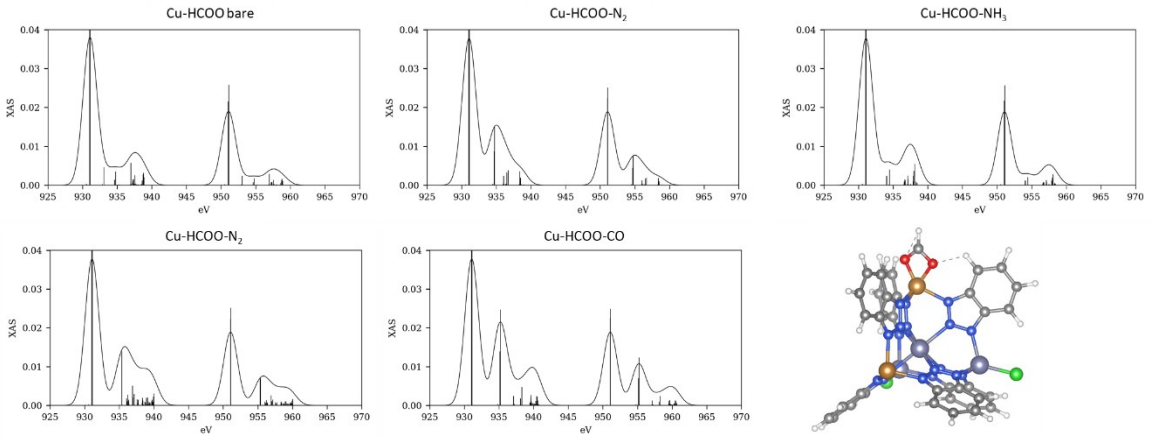

Figure S7. Simulated XAS for two Cu atoms in a cluster with one Cu-HCOO defect and various adsorbed molecules (as for Fig. S4).

Cu^{I}-MFU-4*l* synthesis process

The MOF Cu^{I}-MFU-4*l* studied in our previous work[11] was synthesized with a procedure adapted from that of Denysenko *et al.*[12,13]. The starting point of the reaction is MFU-4*l*, which is constructed from bistriazolate ($BTDD^{2-}$) ligands and $\{Zn_5Cl_4\}^{6+}$ building units. MFU-4*l* is first transformed to Cu^{II}-MFU-4*l* using $CuCl_2$, in which, on average two out of four tetrahedrally coordinated Zn are replaced with Cu^{2+} ions. This is then converted to Cu-MFU-4*l*-formate in a lithium formate in methanol solution. Finally, autoreduction of the Cu^{2+} center to yield Cu^{I}-MFU-4*l* is accomplished by heating the material in vacuo. From the above discussion, we can see that during the synthesis process the tetrahedrally coordinated Cu has been coordinated by Cl and HCOO anions at different steps. If the reaction is not complete, these Cu atoms may keep the Cl and HCOO attached, thereby retaining their 2+ oxidation state in the MOF after the synthesis. Hypothetically, the octahedrally coordinated Zn could be substituted by Cu and leave a Cu^{2+} cation in the center of each Kuratowski unit.

XAS simulation with different exchange-correlation energy functionals:

We employed various hybrid functional with details as follows: M06-2X[14] is a global hybrid functional with 54% Hartree–Fock (HF) exchange; ωB97M-V is a range-separated hybrid, meta-GGA density functional with VV10 nonlocal correlation and 15% short-range exact exchange; The Heyd–Scuseria–Ernzerhof 2006 (HSE06)[15,16] hybrid exchange-correlation functional uses an error-function-screened Coulomb potential to calculate the exchange portion of the energy. It contains 25% of exact exchange up to an intermediate length scale. We also explored some customized functionals based on the PBE0[17,18] functional. PBE0 mixes 25% Hartree–Fock exchange energy in the Perdew–Burke-Ernzerhof (PBE) exchange energy, along with the full PBE correlation energy.

$$E^{PBE0} = \alpha E_x^{HF} + \left(1 - \alpha E_x^{PBE}\right) + E_c^{PBE},$$

where E_x^{HF} is the HF exchange exchange energy, E_x^{PBE} is the PBE exchange energy, and E_c^{PBE} is the PBE correlation energy. In the original PBE0 functional, α is 25 %. In our simulation, we use various values for α: 15%, 20%, and 54%, to see the effect of global HF exchange on the simulated XAS.

The Cu^{2+}/Cu^{+} ratio

Table S2. The Cu^{2+}/Cu^{+} ratio calculated with the MOF cluster attached with Cl, H, HCOO and a Cu_{Zn} defect. The ratio is calculated using Eq. 2. The experimental data from the MOF+CO system, as shown in Fig. 1, were used.

Chemical environment of Cu^{2+}	Cu-Cl	Cu-H	Cu-HCOO	Cu_{Zn}
R(CO)	0.13	0.19	0.12	0.11

The XAS spectra of different structures calculated with the ωB97M-V functional are shown in Fig. 1 with the assumption of fal populations of Cu^{+} (defining the first main peak) and Cu^{2+} (defining the pre-edge peak) based on our molecular cluster models. If the compositional ratio Cu^{2+}/Cu^{+} was 1, then we would expect a pre-edge peak to main peak ratio of $A_{pre}^{sim}/A_{1st}^{sim}$, where we employ peak areas rather than maximal intensities. We define A_{pre}^{exp} and A_{pre}^{sim} as the areas under the pre-edge peak in the experiment and simulation, respectively; and A_{1st}^{exp} and A_{1st}^{sim} as the areas under first main peak in the experiment and simulation, respectively. The actual experimental peak ratio, $A_{pre}^{exp}/A_{1st}^{exp}$ reflects the measured compositional ratio, provided that we renormalize by the theoretical peak ratio. We define the Cu^{2+}/Cu^{+} ratio for adsorbing molecule X as

$$R(X) = A_{pre}^{exp}A_{1st}^{sim}/A_{1st}^{exp}A_{pre}^{sim}. \qquad (2)$$

In the experiment of previous work, CO is expected to occupy all possible Cu^{+} sites, so the Cu^{2+}/Cu^{+} ratio in the MOF is estimated using R(CO) (otherwise an additional contribution from Cu^{+} without adsorbed species should be included). The calculated R(CO) is shown is Table S2. We can see that the average Cu^{2+}/Cu^{+} ratio for different Cu^{2+} defects is close to 0.12. We view Cu-H as an outlier due to its lower chemical stability and likelihood. Its higher ratio estimate results from a relatively weaker pre-edge spectral intensity for Cu^{2+} due to weak orbital mixing between Cu and the attached hydrogen atom.

This quantitative analysis of the mixed-ion population relies explicitly on benchmark estimates of the relative peak intensities of the two oxidation states. By combining predictive theory with experimental measurements, such analysis can be more generally applied to systems with mixed

compositions in various contexts, such as compounds, mixtures, interfaces, etc., that are increasingly accessible using XAS measurements[19–21].

The POSCAR of the primitive cell with one Cu-Cl defect and one Cu-CO group

MOF

1.00000000000000

22.0687999724999990 0.0000000000000000 0.0000000000000000

11.0343999863000004 19.1121414073000011 0.0000000000000000

11.0343999863000004 6.3707138024000001 18.0190997228000001

C Cl Cu H N O Zn

73 5 4 24 36 13 6

Direct

0.4321475134643061 0.0375056811141793 0.0371515017281298

0.4968160360524241 0.0375297855173808 0.0370197314874670

0.0379342242385117 0.4318398323825142 0.0368785197022724

0.0379672579444485 0.4965006426153558 0.0367666380098026

0.4293641543838131 0.4941488720339122 0.0387948587580564

0.4940169519656948 0.4294638884203422 0.0387137241716002

0.3616827970929531 0.0750288181206651 0.0745195511943472

0.4929811236005483 0.0749882675656523 0.0742586149488380

0.0752356205807572 0.3613663269103749 0.0744511021647138

0.0753360401018621 0.4926554166003514 0.0740888902185265

0.3585802207606201 0.4902589549747683 0.0762727758773244

0.4900667770807619 0.3587055761638300 0.0761602755113508

0.3571251905848475 0.1132278258275038 0.1125649277449491

0.4212298461842247 0.1132345057393050 0.1125495877812129

0.1133196261448935 0.3567974562271746 0.1126146987101850

0.1134462885102382 0.4208991448241661 0.1124740262663704

0.3541459088657163 0.4184369455736991 0.1144648430454979

0.4182172487993982 0.3543303448734215 0.1144280735039682

0.1131578231142913 0.4221608133326119 0.3525933416755138

0.4213795598223027 0.1139682939685201 0.3529579602728516

0.1121513124384964 0.1117022431111667 0.3558375820874774

0.0749372457329199 0.4940958770882699 0.3570488810135477

0.4932043648014148 0.0754880246954390 0.3575758779534912

0.0741657394177950 0.0733771823461710 0.3603754141757791

0.1132195551076354 0.3581148847192661 0.4168066826487288

0.3572704000234610 0.1143037186915730 0.4171049199855317

0.1115499675317328 0.1120512257537994 0.4201037559247701

0.0375762002885123 0.4982518250881475 0.4278105940209658

0.4971981025998961 0.0381531826424537 0.4283868362671594

0.0361556199058685 0.0362898215550569 0.4307842554506991

0.0751000387791094 0.3630178776991548 0.4883470336282839

0.3619878036806706 0.0763618855029972 0.4887365656296350

0.0726944881676468 0.0741764794730160 0.4915428704801073

0.0377452982459535 0.4336266978490495 0.4923895779443387

0.4325331201628495 0.0387229758032292 0.4929764575352571

0.0353855710557695 0.0368771593422009 0.4954525036329736

0.5726522416079655 0.9605284751913524 0.5050073603779206

0.9610457353942589 0.5738092892305885 0.5044773426685170

0.9613443014195183 0.9592445362159250 0.5062917577379253

0.6432119920428261 0.9212723234700496 0.5094165489864541

0.9229815655906488 0.6443666018496986 0.5092101702941356

0.9257135055370471 0.9200946384840362 0.5103815510198914

0.5078113626003735 0.9616442346027537 0.5695331381894632

0.9613783664670650 0.5088637168620357 0.5689534061699548

0.9602215802169942 0.9603286387221839 0.5709277182855096

0.6472649665816776 0.8827700962768560 0.5813939713002555

0.8846818283527352 0.6481737635888534 0.5813051074688466

0.8878728583697543 0.8816035722578676 0.5821630335785387

0.5113031856037600 0.9240548686345355 0.6404548805627518

0.9237836868591783 0.5121559630575669 0.6399354291651355

0.9230221473696575 0.9227138463041457 0.6414902593746686

0.5828962633466834 0.8843897171798671 0.6452490996261810

0.8850898696058114 0.5836204018624206 0.6449910661233725

0.8862600014447958 0.8831080205550330 0.6463185661023115

0.8851995280182480 0.6466573530777852 0.8861878263086960

0.8856851570601399 0.5822518519479695 0.8862840059825422

0.5824340694849420 0.8863639529862190 0.8854053045144522

0.6468851259681283 0.8861276849065343 0.8849852095839256

0.6453059928758885 0.5811993588069397 0.8864394550689995

0.5811946504008302 0.6453365757086714 0.8867816475252511

0.9236378637512658 0.6421805009149755 0.9239790460023602

0.9243432760333569 0.5106412444807826 0.9241008983631491

0.5108321857691143 0.9244051441882530 0.9238892636856252

0.6424243733162298 0.9241168380452722 0.9232455772304683

0.6408590649821734 0.5094056313458680 0.9245523853586392

0.5093927777369441 0.6409147141274226 0.9251499799431068

0.9616468649843055 0.5717324237467607 0.9611054036817664

0.9618449927219714 0.5069613260906928 0.9611518485813537

0.5071939509709597 0.9615840596898555 0.9612390733830052

0.5719892639430677 0.9615354404465475 0.9609982375617160

0.5700884799031295 0.5054368021437883 0.9622852257399100

0.5053972934376381 0.5701582940165241 0.9625098061527289

0.8472889426554219 0.8519298333078777 0.8477241069921191

0.5709470280654184 0.1466716106809988 0.1403505960625074

0.1458456916993102 0.5711193021931330 0.1398559798366208

0.8581558610068512 0.4309138556879953 0.8540066880664615

0.4308626495121999 0.8572308594340482 0.8558535236439255

0.8487192432462459 0.8674981140099339 0.4351828481257023

0.1897591934377604 0.1895855969060185 0.1894192101841862

0.1896608523733625 0.1899730226231535 0.4309144087051098

0.8165231261980506 0.8135384550349082 0.5528561325442012

0.8160776505490288 0.8158872297907159 0.8154234081861417

0.3132317891262184 0.0740592930148654 0.0737223348702156

0.5430157455157290 0.0744358769322368 0.0735746095178751

0.0742538764366144 0.3129146013718911 0.0736654204482754

0.0748326967230311 0.5426767602170530 0.0733840994819218

0.3096656419282681 0.5401952829959827 0.0758003906450352

0.5399592023194437 0.3097437004302293 0.0756190238604019

0.0743858456695182 0.5439925523773519 0.3080838957079612

0.5432230684252385 0.0745782202477992 0.3087421241123873

0.0738015216915813 0.0720737432806570 0.3118661077534207

0.6923619559205527 0.9211098343849272 0.4597443238832609

0.9232919031359836 0.6934717692033949 0.4594740263075622

0.9266637077212414 0.9200652330248468 0.4605120808182284

0.0741520270602117 0.3147490188356039 0.5387430195549661

0.3136077316575593 0.0757894188084843 0.5390305252543045

0.0709999293742026 0.0734806437432355 0.5420600601381025

0.4612304843763314 0.9256185920700297 0.6891884871434750

0.9246017739766029 0.4620017662689528 0.6886042938167032

0.9230160120155217 0.9248075635409011 0.6897786953535445

0.9243785899773410 0.6906896271367695 0.9249399090328374

0.9251261641541090 0.4605316879604405 0.9247099039026202

0.4607144871256166 0.9249899040005470 0.9247138323308121

0.6908844244636487 0.9250116715167549 0.9241256816948608

0.6897414913067103 0.4594531175859259 0.9248672380108970

0.4594780430537797 0.6898378516994539 0.9258499057673638

0.2971612823292539 0.1547462055977125 0.1541825732380843

0.3969876052647460 0.1550052325929320 0.1544789047818171

0.1546766856679911 0.2968537392396768 0.1543984792367752

0.1551554893476755 0.3966837755009820 0.1544374937635643

0.2945047302696484 0.3944268187864611 0.1563468762928877

0.3941460172310161 0.2947239812512843 0.1562929411210766

0.3224021879198942 0.1791222324589765 0.1787437716602858

0.1791134820169807 0.3221082548357573 0.1788910513428582

0.3199081618356968 0.3201727107081229 0.1807636090886944

0.1549037931026925 0.3976694871294672 0.2932771885686495

0.3970820877577214 0.1555462776835681 0.2935343487559436

0.1539980575158498 0.1530744717430866 0.2962276231762237

0.1790709782781398 0.3230845777632000 0.3196704927763193

0.3224898619751173 0.1798933089531604 0.3197725866980826

0.1778852058537840 0.1775380661488732 0.3223917172806377

0.1547262217021433 0.2979631812271397 0.3938708612522073

0.2972546912715614 0.1558036945756622 0.3939825964473988

0.1530869424220308 0.1535647541415306 0.3969789775293644

0.7067354416919682 0.8396638514650659 0.6057270699675745

0.8423051158360995 0.7071959545122115 0.6064909252221440

0.8471303901680649 0.8386873676267340 0.6062581172378295

0.6806972139131119 0.8164081632969878 0.6799184293305891

0.8182126337792753 0.6807714216479993 0.6806406565837039

0.8219287958769845 0.8158101214718846 0.6807069121400432

0.6064617058617620 0.8423899330566003 0.7051384169114749

0.8430805412373230 0.6067412983576778 0.7051810006322417

0.8445743964520650 0.8415008063679976 0.7063532164066805

0.8187027235700793 0.6805175005470619 0.8211144575313049

0.6805981883686016 0.8206338320613272 0.8189706314526707

0.6794430239555418 0.6794658797522439 0.8203420166150016

0.8428761985629243 0.7064526094127073 0.8449634007309691

0.8435155956753879 0.6060190141322436 0.8449650348981603

0.6061081075700807 0.8448033975113520 0.8435184599772446

0.7066278151011408 0.8445502699643781 0.8429873202022290

0.7049498778906430 0.6052309854387528 0.8444352281229112

0.6052389698003774 0.7049711242218629 0.8449943050623318

0.4372735006980688 0.9994832043083389 0.9995542515683774

0.5668609619427517 0.9992263496039788 0.9988987170564778

0.0002112300722848 0.4370131218746001 -0.0010407811288803

0.9998429718479523 0.5665617843661657 0.9985194734489420

0.4352907493160366 0.5643184921817884 0.0007010509114308

0.5642128825520705 0.4353491864352797 0.0004569736864087

0.9993457914994640 0.5683941284600490 0.4341526898184891

0.5672063631734394 -0.0004332368047912 0.4346630867119942

0.9983791840146233 0.9982811729712679 0.4361708870438512

0.0001090565768367 0.4389995284674085 0.5627594559136003

0.4378733367823252 0.0012976310541017 0.5633449559914065

0.9964459552395273 -0.0002663572105581 0.5656240383145972

0.8652658675931645 0.8769080839920212 0.8684506876435253

0.4501791434718510 0.1840397919810220 0.1829457421177647

0.1838949799955191 0.4503318126748148 0.1825828723777895

0.2488434877254110 0.2487973062861404 0.2514193189367758

0.7496952914588439 0.7504041063060647 0.7512768633486294

0.5515919114772680 0.8161905833727611 0.8159609070458913

0.8159630095890489 0.5515731060163743 0.8163901055516567

References:

(1) Kresse, G.; Furthmüller, J. Efficiency of Ab-Initio Total Energy Calculations for Metals and Semiconductors Using a Plane-Wave Basis Set. *Comput. Mater. Sci.* **1996**, *6* (1), 15–50. https://doi.org/http://dx.doi.org/10.1016/0927-0256(96)00008-0.

(2) Kresse, G.; Furthmüller, J. Efficient Iterative Schemes for Ab Initio Total-Energy Calculations Using a Plane-Wave Basis Set. *Phys. Rev. B* **1996**, *54* (16), 11169–11186. https://doi.org/10.1103/PhysRevB.54.11169.

(3) Kresse, G.; Joubert, D. From Ultrasoft Pseudopotentials to the Projector Augmented-Wave Method. *Phys. Rev. B* **1999**, *59* (3), 1758–1775. https://doi.org/10.1103/PhysRevB.59.1758.

(4) Blöchl, P. Projector Augmented-Wave Method. *Phys. Rev. B* **1994**, *50* (24), 17953.

(5) Lee, K.; Murray, É. D.; Kong, L.; Lundqvist, B. I.; Langreth, D. C. Higher-Accuracy van Der Waals Density Functional. *Phys. Rev. B* **2010**, *82* (8), 81101. https://doi.org/10.1103/PhysRevB.82.081101.

(6) Mann, G. W.; Lee, K.; Cococcioni, M.; Smit, B.; Neaton, J. B. First-Principles Hubbard U Approach for Small Molecule Binding in Metal-Organic Frameworks. *J. Chem. Phys.* **2016**, *144* (17), 174104. https://doi.org/10.1063/1.4947240.

(7) Weigend, F.; Ahlrichs, R. Balanced Basis Sets of Split Valence{,} Triple Zeta Valence and Quadruple Zeta Valence Quality for H to Rn: Design and Assessment of Accuracy. *Phys. Chem. Chem. Phys.* **2005**, *7* (18), 3297–3305. https://doi.org/10.1039/B508541A.

(8) Besley, N. A. Calculation of the Electronic Spectra of Molecules in Solution and on Surfaces. *Chem. Phys. Lett.* **2004**, *390* (1), 124–129. https://doi.org/https://doi.org/10.1016/j.cplett.2004.04.004.

(9) Dreuw, A.; Head-Gordon, M. Single-Reference Ab Initio Methods for the Calculation of Excited States of Large Molecules. *Chem. Rev.* **2005**, *105* (11), 4009–4037. https://doi.org/10.1021/cr0505627.

(10) Shao, Y.; Gan, Z.; Epifanovsky, E.; Gilbert, A. T. B.; Wormit, M.; Kussmann, J.; Lange, A. W.; Behn, A.; Deng, J.; Feng, X.; Ghosh, D.; Goldey, M.; Horn, P. R.; Jacobson, L. D.; Kaliman, I.; Khaliullin, R. Z.; Kuś, T.; Landau, A.; Liu, J.; Proynov, E. I.; Rhee, Y. M.; Richard, R. M.; Rohrdanz, M. A.; Steele, R. P.; Sundstrom, E. J.; III, H. L. W.; Zimmerman, P. M.; Zuev, D.; Albrecht, B.; Alguire, E.; Austin, B.; Beran, G. J. O.; Bernard, Y. A.; Berquist, E.; Brandhorst, K.; Bravaya, K. B.; Brown, S. T.; Casanova, D.; Chang, C.-M.; Chen, Y.; Chien, S. H.; Closser, K. D.; Crittenden, D. L.; Diedenhofen, M.; Jr., R. A. D.; Do, H.; Dutoi, A. D.; Edgar, R. G.; Fatehi, S.; Fusti-Molnar, L.; Ghysels, A.; Golubeva-Zadorozhnaya, A.; Gomes, J.; Hanson-Heine, M. W. D.; Harbach, P. H. P.; Hauser, A. W.; Hohenstein, E. G.; Holden, Z. C.; Jagau, T.-C.; Ji, H.; Kaduk, B.; Khistyaev, K.; Kim, J.; Kim, J.; King, R. A.; Klunzinger, P.; Kosenkov, D.; Kowalczyk, T.; Krauter, C. M.; Lao, K. U.; Laurent, A. D.; Lawler, K. V; Levchenko, S. V; Lin, C. Y.; Liu, F.; Livshits, E.; Lochan, R. C.; Luenser, A.; Manohar, P.; Manzer, S. F.; Mao, S.-P.; Mardirossian, N.; Marenich, A. V; Maurer, S. A.; Mayhall, N. J.; Neuscamman, E.; Oana, C. M.; Olivares-Amaya, R.; O'Neill, D. P.; Parkhill, J. A.; Perrine, T. M.; Peverati, R.; Prociuk, A.; Rehn, D. R.; Rosta, E.; Russ, N. J.; Sharada, S. M.; Sharma, S.; Small, D. W.; Sodt, A.; Stein, T.; Stück, D.; Su, Y.-C.; Thom, A. J. W.; Tsuchimochi, T.; Vanovschi, V.; Vogt, L.; Vydrov, O.; Wang, T.; Watson, M. A.; Wenzel, J.; White, A.; Williams, C. F.; Yang, J.; Yeganeh, S.; Yost, S. R.; You, Z.-Q.; Zhang, I. Y.; Zhang, X.; Zhao, Y.; Brooks, B. R.; Chan, G. K. L.; Chipman, D. M.; Cramer, C. J.; III, W. A. G.; Gordon, M. S.; Hehre, W. J.; Klamt, A.; III, H. F. S.; Schmidt, M. W.; Sherrill, C. D.; Truhlar, D. G.; Warshel, A.; Xu, X.; Aspuru-Guzik, A.; Baer, R.; Bell, A. T.; Besley, N. A.; Chai, J.-D.; Dreuw, A.; Dunietz, B. D.; Furlani, T. R.; Gwaltney, S. R.; Hsu, C.-P.; Jung, Y.; Kong, J.; Lambrecht, D. S.; Liang, W.; Ochsenfeld, C.; Rassolov, V. A.; Slipchenko, L. V; Subotnik, J. E.; Voorhis, T. Van; Herbert, J. M.; Krylov, A. I.; Gill, P. M. W.; Head-Gordon, M. Advances in Molecular Quantum Chemistry Contained in the Q-Chem 4 Program Package. *Mol. Phys.* **2015**, *113* (2), 184–215. https://doi.org/10.1080/00268976.2014.952696.

(11) Su, G. M.; Wang, H.; Barnett, B. R.; Long, J. R.; Prendergast, D.; Drisdell, W. S. Backbonding Contributions to Small Molecule Chemisorption in a Metal–Organic Framework with Open Copper(i) Centers. *Chem. Sci.* **2021**, *12* (6), 2156–2164. https://doi.org/10.1039/D0SC06038K.

(12) Denysenko, D.; Grzywa, M.; Jelic, J.; Reuter, K.; Volkmer, D. Scorpionate-Type Coordination in MFU-4l Metal–Organic Frameworks: Small-Molecule Binding and Activation upon the Thermally Activated Formation of Open Metal Sites. *Angew. Chemie Int. Ed.* **2014**, *53* (23), 5832–5836. https://doi.org/https://doi.org/10.1002/anie.201310004.

(13) FitzGerald, S. A.; Mukasa, D.; Rigdon, K. H.; Zhang, N.; Barnett, B. R. Hydrogen Isotope Separation within the Metal–Organic Framework Cu(I)-MFU-4l. *J. Phys. Chem. C* **2019**, *123* (50), 30427–30433. https://doi.org/10.1021/acs.jpcc.9b09332.

(14) Zhao, Y.; Truhlar, D. G. The M06 Suite of Density Functionals for Main Group Thermochemistry, Thermochemical Kinetics, Noncovalent Interactions, Excited States, and Transition Elements: Two New Functionals and Systematic Testing of Four M06-Class Functionals and 12 Other Function. *Theor. Chem. Acc.* **2008**, *120* (1), 215–241. https://doi.org/10.1007/s00214-007-0310-x.

(15) Henderson, T. M.; Janesko, B. G.; Scuseria, G. E. Generalized Gradient Approximation Model Exchange Holes for Range-Separated Hybrids. *J. Chem. Phys.* **2008**, *128* (19), 194105. https://doi.org/10.1063/1.2921797.

(16) Krukau, A. V; Vydrov, O. A.; Izmaylov, A. F.; Scuseria, G. E. Influence of the Exchange Screening Parameter on the Performance of Screened Hybrid Functionals. *J. Chem. Phys.* **2006**, *125* (22). https://doi.org/10.1063/1.2404663.

(17) Adamo, C.; Barone, V. Toward Reliable Density Functional Methods without Adjustable Parameters: The PBE0 Model. *J. Chem. Phys.* **1999**, *110* (13), 6158–6170. https://doi.org/10.1063/1.478522.

(18) Perdew, J. P.; Ernzerhof, M.; Burke, K. Rationale for Mixing Exact Exchange with Density Functional Approximations. *J. Chem. Phys.* **1996**, *105* (22), 9982–9985. https://doi.org/10.1063/1.472933.

(19) Nie, K.; Zhang, H.; McLeod, J. A.; Zhang, D.; Zhou, D.; Xia, Y.; Zhong, J.; Liao, L.; Guo, J.; Sun, X. Real-Time Interface Investigation on Degradation Mechanism of Organic Light-Emitting Diode by in-Operando X-Ray Spectroscopies. *Org. Electron.* **2020**, *87*, 105901. https://doi.org/https://doi.org/10.1016/j.orgel.2020.105901.

(20) Xiao, W.; Sun, Q.; Liu, J.; Xiao, B.; Li, X.; Glans, P.-A.; Li, J.; Li, R.; Li, X.; Guo, J.; Yang, W.; Sham, T.-K.; Sun, X. Engineering Surface Oxygenated Functionalities on Commercial Carbon toward Ultrafast Sodium Storage in Ether-Based Electrolytes. *ACS Appl. Mater. Interfaces* **2020**, *12* (33), 37116–37127. https://doi.org/10.1021/acsami.0c08899.

(21) Liu, Y.-S.; Feng, X.; Glans, P.-A.; Guo, J. In-Situ/Operando Soft x-Ray Spectroscopy Characterization of Energy and Catalytic Materials. *Sol. Energy Mater. Sol. Cells* **2020**, *208*, 110432. https://doi.org/https://doi.org/10.1016/j.solmat.2020.110432.